Nano-morphology induced additional surface plasmon resonance enhancement of SERS sensitivity in Ag/GaN nanowall network

2015 Nanotechnology 26 465701

(http://iopscience.iop.org/0957-4484/26/46/465701)

IOP Publishing Nanotechnology
Nanotechnology 26 (2015) 465701 (7pp) doi:10.1088/0957-4484/26/46/465701

Nano-morphology induced additional surface plasmon resonance enhancement of SERS sensitivity in Ag/GaN nanowall network

S Sharvani[1], Kishor Upadhayaya[2], Gayatri Kumari[1], Chandrabhas Narayana[1] and S M Shivaprasad[1]

[1] Chemistry and Physics of Materials Unit, Jawaharlal Nehru Centre for Advanced Scientific Research, Bangalore-560064, India
[2] Thin Films Lab, B.V. Bhoomaraddi College of Engineering and Technology, Hubballi-580031, India

E-mail: smsprasad@jncasr.ac.in

Received 24 August 2015, revised 30 September 2015
Accepted for publication 30 September 2015
Published 26 October 2015

Abstract

The GaN nanowall network, formed by opening the screw dislocations by kinetically controlled MBE growth, possesses a large surface and high conductivity. Sharp apexed nanowalls show higher surface electron concentration in the band-tail states, in comparison to blunt apexed nanowalls. Uncapped silver nanoparticles are vapor deposited on the blunt and sharp GaN nanowall networks to study the morphological dependence of band-edge plasmon-coupling. Surface enhanced Raman spectroscopy studies performed with a rhodamine 6G analyte on these two configurations clearly show that the sharp nanowall morphology with smaller Ag nanoparticles shows higher enhancement of the Raman signal. A very large enhancement factor of 2.8×10^{7} and a very low limit of detection of 10^{-10} M is observed, which is attributed to the surface plasmon resonance owing to the high surface electron concentration on the GaN nanowall in addition to that of the Ag nanoparticles. The significantly higher sensitivity with same-sized Ag nanoparticles confirms the unconventional role of morphology-dependent surface charge carrier concentration of GaN nanowalls in the enhancement of Raman signals.

Keywords: GaN, SERS, Ag nanoparticles

(Some figures may appear in colour only in the online journal)

1. Introduction

Of late, Raman and infrared (IR) spectroscopy have assumed great importance as tools in the detection of proteins [1, 2], viruses [3], bacteria [4], cancer [5] cells in tissues, etc. Though conventional Raman spectroscopy provides molecular fingerprinting information, it suffers a major drawback owing to its very low cross-sectional scattering and low incident photon flux [6]. Surface enhanced Raman spectroscopy (SERS) has emerged as a new tool to obtain a million times enhanced Raman signal by using plasmonic nanostructures [7]. Metal nanoparticles deposited on a substrate support localized surface plasmons due to collective oscillation of their surface free electrons [8] upon excitation by electromagnetic radiation. The surface plasmon resonance (SPR) of metal nanoparticles which form 'hotspots' can be tuned by tailoring their size and shape [9, 10]. Nanorods, nanostars, nanoshells, core–shell nanoparticles, chains and other nano-architectures show interesting optical properties which have been harnessed to improve the SERS signal [11–14]. In addition to this, the refractive index of the surrounding medium also plays a significant role in determining SPR [15, 16]. The past few decades have witnessed an upsurge in research on metal nanoparticles for achieving higher SERS enhancement factors and low-detection limits. A uniform distribution of the hotspots, and an increased surface area of

substrates will provide reliable and quantifiable enhancement [17, 18]. There are several studies in the literature on planar surfaces which focus on optimizing the conditions to obtain very high enhancement factors and detection of very low concentration of analytes [19] and include roughening of the surfaces of metal nanoparticles for increased adhesion of analyte molecules. Depositing capped nanoparticles on functionalized substrates, growing nanostructures by lithography, physical vapor deposition, etc, are a few of the techniques that are employed to obtain uniform arrays of nanoparticles [20]. Wang *et al* [21] have shown that surfactantless growth of various silver nanostructures on p-type and n-type GaN substrate can enhance the signal. Nie *et al* [22] have demonstrated that Ag on nanoporous GaN thin films exhibit enhanced SERS in comparison to Ag on planar GaN. Dar *et al* [23] showed a composite structure made of Ag nanoparticles adsorbed on GaN nanorods exhibiting SERS. All these attempts focus on searching for a substrate system that has a large surface area and a uniform distribution of uncapped metal nanoparticles, for quantitative and reliable detection of bio-molecules using SERS. But studies related to the role of morphology-dependent optoelectronic properties of the substrate supporting the nanoparticles in the SERS mechanism have been scarce.

Recently, we have developed a novel high surface area GaN nanowall network substrate uniformly covered with plasmonic Ag nano-droplets. This can be employed as a highly sensitive and charge independent SERS substrate, for label-free bio-molecule detection [24]. This substrate, with unique morphology and electronic structure, was shown to be stable and re-useable and resulted in better enhancement of electric field than with conventional substrates like silicon. In this paper, we show a further enhancement of Raman signal intensity from Ag deposited on a particular morphology of GaN nanowall network which possesses a large density of band-tail states on the surface of GaN nanowall and an optimal size of adsorbed Ag nanoparticles. Here, we have investigated the change in SERS enhancement factor as a function of the size of adsorbed silver nanoparticles on a GaN network of two morphologies that possess different densities of band-tail states. We report here high values of enhancement factor (EF) along with a very low limit of detection (LOD) for rhodamine (R6G) molecules, with 13 nm Ag nanoparticles adsorbed on GaN networks with sharp apexes due to increased surface area and additional plasmon resonance from free surface electrons in the band-tail states.

2. Methods

C-plane sapphire [Al_2O_3 (0001)] was used as the substrate for the growth of nanostructured gallium nitride films by molecular beam epitaxy (SVT Assoc., USA) at a base pressure of 3×10^{-11} Torr. Prior to the growth, sapphire substrates were cleaned via chemical treatment, degassed at 500 °C in the preparation chamber at 1×10^{-9} Torr vacuum for 60 min, and then again degassed in ultra-high vacuum (3×10^{-11} torr) in the growth chamber for 30 min at 800 °C temperature. A typical streaky RHEED pattern was observed to ascertain an atomically clean substrate surface before commencing growth under optimized nitrogen rich conditions (III-V ratio 1:100) to obtain the nanowall network morphology whose growth details are provided elsewhere [25]. Substrate temperatures of 630 °C and 680 °C were employed for growth times of 3 h and 4 h to obtain the blunt and sharp network morphologies, respectively. N_2 gas flow rate was maintained at 4.5 sccm with a RF forward power of 375 W, and the temperature of the Ga Knudsen cell was kept at 1000 °C. A physical vapor deposition system (PVD) operating at a base pressure of 1.0×10^{-9} Torr was used to deposit Ag (99.99% wire from Alfa Aesar) nanoparticles of desired coverage and size by electron beam evaporation on both the blunt and sharp GaN networks. A quartz crystal microbalance was used to monitor the coverage of Ag deposited on the substrate. The morphology and particle size distribution of the samples were analyzed by employing the Imagej software. These films were then characterized *ex situ* by several complimentary techniques. Field emission scanning electron microscope (Quanta 3D FEG, FEI, Netherlands) images were acquired at different magnifications at an operating voltage of 20 kV. X-ray photoelectron spectroscopy (ESCA+, Omicron Nanotechnology, Germany) was performed on all the samples using a Mg K_α anode with a pass energy of 25 eV and 10 eV for core-level and valance band scans, respectively. Emission studies of the GaN films were performed by a photoluminescence instrument (HORIBA Scientific, Japan) using a helium–cadmium laser with a power of 27–30 mW and 325 nm excitation.

Raman and SERS spectra were recorded in the 180° backscattering geometry, using a 532 nm excitation from a diode pumped frequency doubled Nd:YAG solid state laser (model GDLM-5015 L, Photop Suwtech Inc.) with a custom-built Raman spectrometer equipped with a SPEX TRIAX 550 monochromator and a liquid nitrogen cooled CCD (Spectrum One with CCD 3000 controller, ISA Jobin Yvon). Laser power at the sample was ~8 mW, and the typical spectral acquisition time was 30 s. For acquiring SERS spectra, 1 μl of different concentrations of R6G were drop-cast on the substrates and dried for a minimum of 1 h before recording the Raman spectrum.

3. Results and discussion

To obtain appropriate the SERS substrate, Ag of two sizes, 13 nm and 25 nm, was deposited on the blunt and sharp morphological manifestations of GaN nanowall network. Figure 1 shows FESEM images before and after deposition of Ag with different coverages on the two different GaN network morphologies. Figure 1(a) shows the bare sharp apexed and figure 1(d) the bare blunt apexed nanowalls. This network forms as a result of formation of open screw dislocations which is a misfit strain relaxation pathway of the interfacial misfit stress developed between the GaN film and the sapphire substrate which have a lattice mismatch of ≈16% [26]. From the line-scans of the figures it is clear that the average width of tips (apex) of the sharp network (figure 1(a)) is <10 nm,

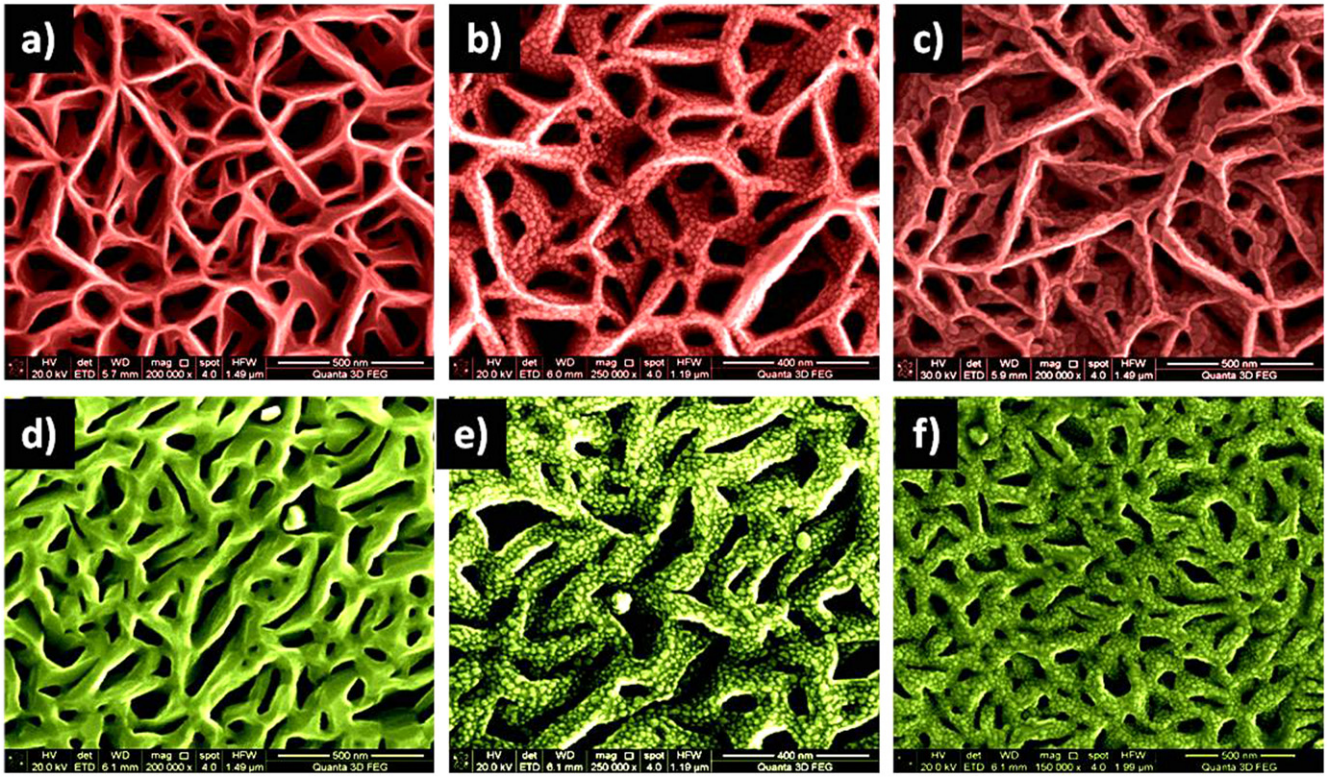

Figure 1. FESEM images of the GaN nanowall network at different Ag coverages: (a) GaNS, (b) AgS13, (c) AgS25, (d) GaNB, (e) AgB13, (f) AgB25.

while the average width of the apex is 50–60 nm for the blunt network (figure 1(d)). The respective surface areas were geometrically estimated from the FESEM images and were 70 $m^2\,gms^{-1}$ and 80 $m^2\,gms^{-1}$ for blunt and sharp networks, respectively, and thus only 10% different. The particle size distribution (PSD) (figure 2) shows the size variations of Ag nanoparticles on the sharp (a and b) and on the blunt (c and d) networks. The average size of Ag nanoparticles is 13 nm in the first (figures 2(a) and (c)) and 25 nm for the second coverage (figures 2(b) and (d)). Another sample (not shown here) was deposited with a high Ag coverage, so that the entire GaN surface was covered by Ag particles of size larger than 100 nm.

The sample nomenclature assigned in this paper is as follows: GaNS—sharp GaN nanowall network; GaNB—blunt GaN nanowall network; AgS13 and AgS25— silver NP of diameter 13 nm and 25 nm, respectively, deposited on the sharp GaN network; AgB13 and AgB25—silver NP of diameter 13 nm and 25 nm, respectively.

Figure 3(a) is the room temperature photoluminescence spectra showing the band-edge emission of GaN (without Ag deposition) from the bare sharp and blunt nanowall networks, compared with that of a 2μm thick flat GaN epilayer sample. PL emission of the flat GaN epilayer film is less intense and possesses a narrower FWHM compared to that of GaN nanowall network, due to the non-radiative defect states. The high intensity in nanowalls is attributed to the defect and strain-free nature of the walls, while the broad FWHM is due to the high density of band-tail states in the conduction band at room temperature due to surface states. [27] The blunt nanowall network (GaNB) sample displays two times higher photoemission intensity and three times broader FWHM in comparison to the flat epilayer. The band-edge emission at ~360 nm in the case of the sharp morphological network (GaNS) is further enhanced by about a four times increase in intensity and six times increase in FWHM in comparison to the flat epilayer due to geometry induced optical confinement in the cavities of diameter ~150 nm. Measurements of the areas under the curves show a photoluminescence enhancement of four times in the blunt network sample and 15 times for the sharp configuration, compared to the emission obtained from the flat GaN epilayer. The PL peak is also seen to be blue shifted by ~100 meV which can be attributed to electron confinement in the narrow regions of the apex of the nanowall, which are comparable to the excitonic radius of GaN (11 nm). In contrast to the high resistance of the GaN epilayer, the GaN nanowall network is seen to be highly conducting. The sharp and blunt nanowall networks are found to have electron concentrations of $10^{20}\,cm^{-3}$ and $10^{18}\,cm^{-3}$, respectively, by Hall measurements. The nanowall structure has been modeled in our previous paper, based on which we estimate the volume and consequently the electron concentration. These values have also been verified by thermoelectric measurements [27].The enhancement of the PL signal in the nanowall network (especially in the sharp one), even at low temperatures and high carrier concentration, conductivity and high Stokes's shift suggest the presence of a high density of band-tail states in the electronic structure of these defects

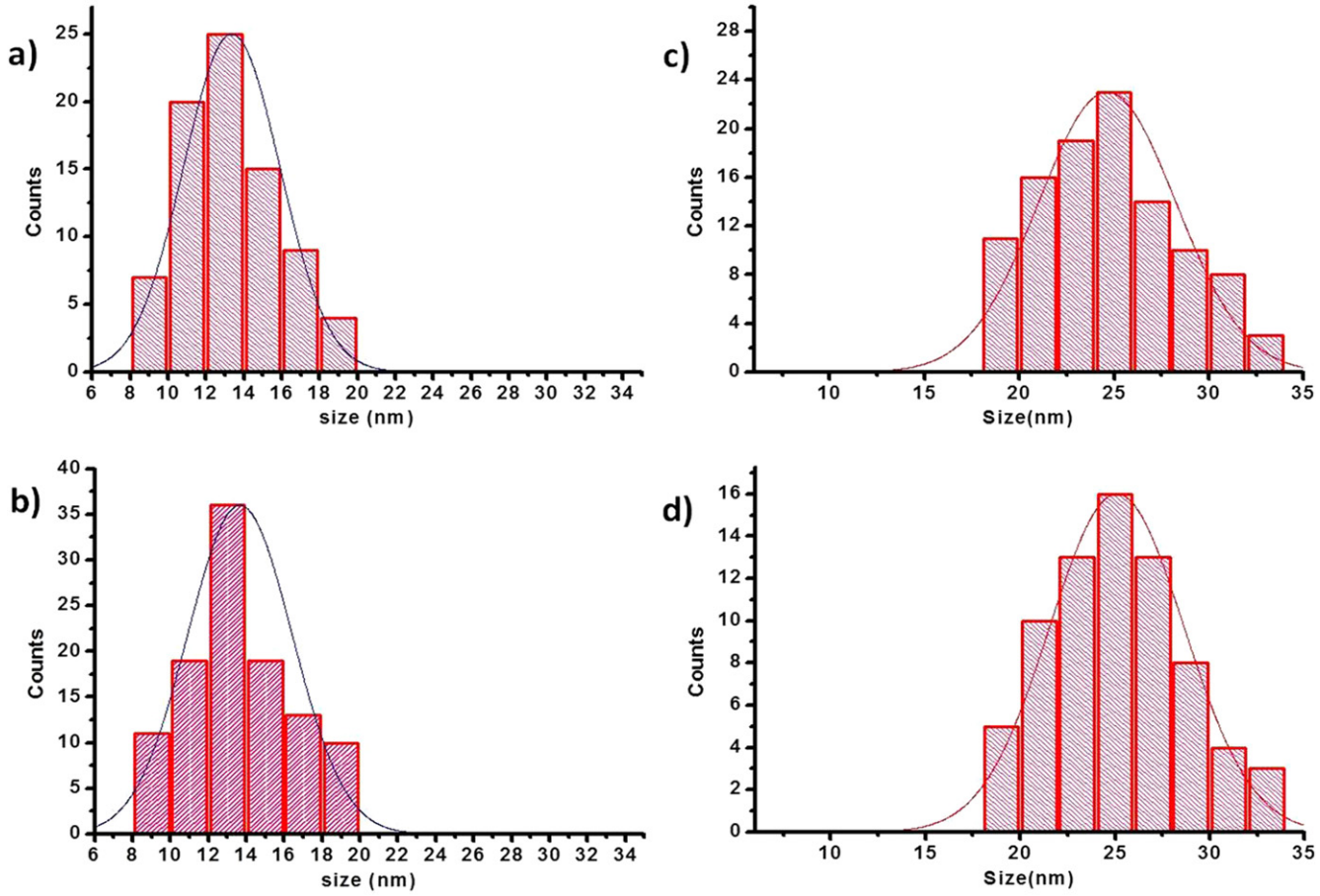

Figure 2. Particle size distribution (PSD) of all the substrates (a) AgS13, (b) AgB13, (c) AgS25, (d) AgB25.

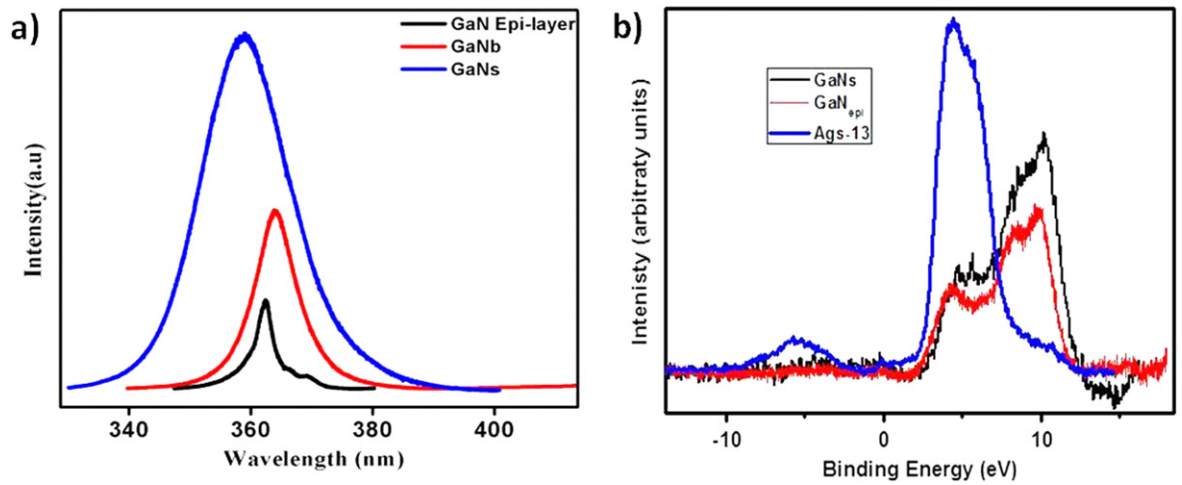

Figure 3 (a) Photoluminescence and (b) XPS spectra of GaN epilayer, blunt nanowall network (GaNB) of GaN and sharp (GaNS) nanowall network of GaN.

and strain-free, single crystalline morphologies [28]. To probe the valence band electron occupation, we have performed x-ray photoelectron spectroscopy (XPS) measurements in the low binding-energy region, shown in figure 3(b) for the GaN epilayer, the sharp nanowall network (GaNS) and when GaNS is covered with Ag nanoparticles. A strong Ag (3d) peak appears at ∼5 eV for the AgS13 sample due to the the deposition of silver, while the valence band spectra for the epilayer and the nanowall network appear qualitatively similar. An additional peak at −5 eV observed for the sharp nanowall network sample is attributed to the presence of a high density of electrons in the conduction band of this morphology, originating from nitrogen vacancies on the surface of the nanowalls. Thus, in addition to the optical

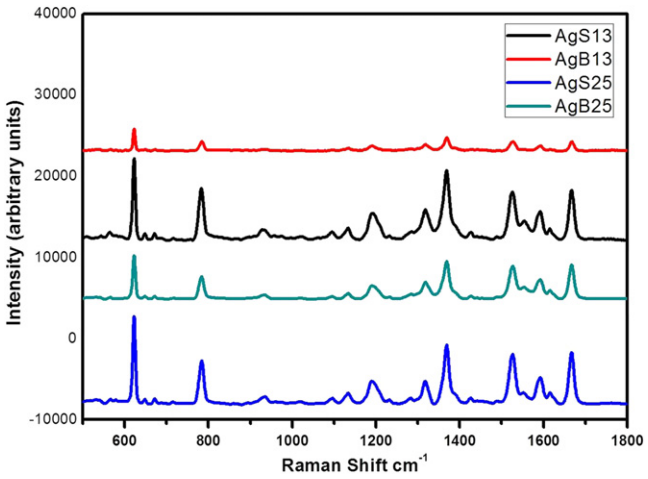

Figure 4. SERS spectra of 10^{-5} M rhodamine 6G on AgB13 nm, AgS13 nm, AgB25 nm and AgS25 nm.

confinement and large area effects, the contribution from surface electrons enhances the emission properties of their nano-manifestation.

Raman studies. We have measured Raman signals for the five Ag deposited substrates using rhodamine 6G as the analyte molecule. To investigate the role of silver nanoparticles on sharp and blunt GaN nanowalls on their respective SERS enhancement factor, rhodamine (R6G) was drop-cast on bare GaN and Ag deposited GaN substrates. Raman spectra acquired for 10^{-5} M concentration of R6G on bare sharp and blunt GaN samples and also on the two silver deposited GaN substrates are shown in figure 4. The SERS signal acquired for bare samples was very weak, whereas for the Ag deposited GaN substrates the intensity was strong as expected from the literature [18, 29]. It can also be clearly seen that silver on sharp GaN nanowalls show higher SERS enhancement when compared with that of Ag on blunt GaN nanowalls. Among the two Ag NP sizes on the sharp GaN network, the 13 nm Ag particles showed higher Raman enhancement than with 25 nm Ag nanoparticles. Experiments were also performed on GaN network with Ag particles larger than 100 nm (not shown here) which showed very weak Raman peak intensities due to the lack of hotspots required for surface plasmon resonance.

The increase in the Raman signal is quantified by the enhancement factor (G) which is given as:

$$\mathbf{G} = (\mathbf{I_{SERS}}/\mathbf{I_{NORM}})\,(\mathbf{N_{BULK}}/\mathbf{N_{SERS}}) \quad (1)$$

where I_{SERS} and I_{NORM} are the respective intensities of a specific band in SERS and normal Raman spectra of the analyte molecule. N_{BULK} and N_{SERS} are the number of molecules probed under the illumination of the laser beam in bulk and SERS experiments, respectively.

N_{SERS} is given by C × A, where *C* is the surface density of rhodamine (5.8×10^{12} molecules cm^{-2}) and *A* is the laser spot area. N_{BULK} is given by $(A \times h \times \rho)/m$, where *h*, ρ, and *m* are the penetration depth, the density (1.26 g cm^{-3}), and the molecular weight (479.02 g mol^{-1}) of rhodamine G6, respectively. It is clear from figure 4 and table 1 that when we compare the enhancement for same-sized Ag nanoparticles deposited on the blunt and sharp nanowalls, sharp nanowalls yield higher enhancements, owing to the higher surface electron concentration. It is interesting to observe that the signals from both AgS13 and AgS25 are almost similar, whereas the signal from AgB25 increases two-fold compared to that from AgB13. This can be explained by considering enhancement of the Raman signals as a combined effect arising from the size distribution of the Ag nanoparticles as well as the surface electron concentration of GaN nanowalls. In case of blunt samples (AgB13 and AgB25) the distribution of hotspots mainly depends upon the distribution of Ag nanoparticles, since the surface electron concentration is relatively lower. Therefore, as the size of Ag nanoparticles increases, the hot-spot density increases, which in turn increases the number of adsorbed molecules on the sample and hence the enhancement in the Raman signal. In the case of sharp samples, the distribution of hotspots is due to combination of surface free electrons from both the sharp apex of GaN and Ag nanoparticles. As the size of nanoparticles increases from 13 nm to 25 nm the free electron distribution on the surface of the sample remains almost same and hence there is not much change in the enhancement they produced. Figure 5 shows the Raman signal obtained on the four samples (AgS13, AgB13, AgS25 and AgB25) for different concentrations varying from 10^{-4} M to 10^{-10} M of the analyte molecules to determine the detection sensitivity and limit of detection in each case. The Raman signal is observable up to a low concentration of 10^{-10} M for samples AgS13 and AgS25, while the other two samples AgB13 and AgB25 show lower LODs of 10^{-7} M and 10^{-9} M, respectively. The respective LOD values are also listed in table 1.

Table 1. SERS enhancement factor and limit of detection of R6G for all the substrates.

Substrate	Enhancement factor	Limit of detection (M)
AgS13 nm	2.7×10^7	10^{-10}
AgS25 nm	2.8×10^7	10^{-10}
AgB13 nm	1×10^6	10^{-7}
AgB25 nm	1.9×10^6	10^{-9}

4. Conclusions

GaN with two different nanowall network morphologies have been studied here, and it is evident that the sharp nanowall network possesses a high density of band-tail states that results in a much enhanced band-edge emission and carrier concentration compared to the blunt nanowall network and flat epilayer. These two morphologies coated with Ag nanoparticles of different sizes were used as the SERS substrate with R6G of different concentrations as the analyte. The sharp nanowall network exhibits a high enhancement factor of $\sim 10^7$ and low LOD of 10^{-10} M of Raman signals than the blunt nanowall network which is attributed to its higher density of surface charge carriers in the conduction band. This is in

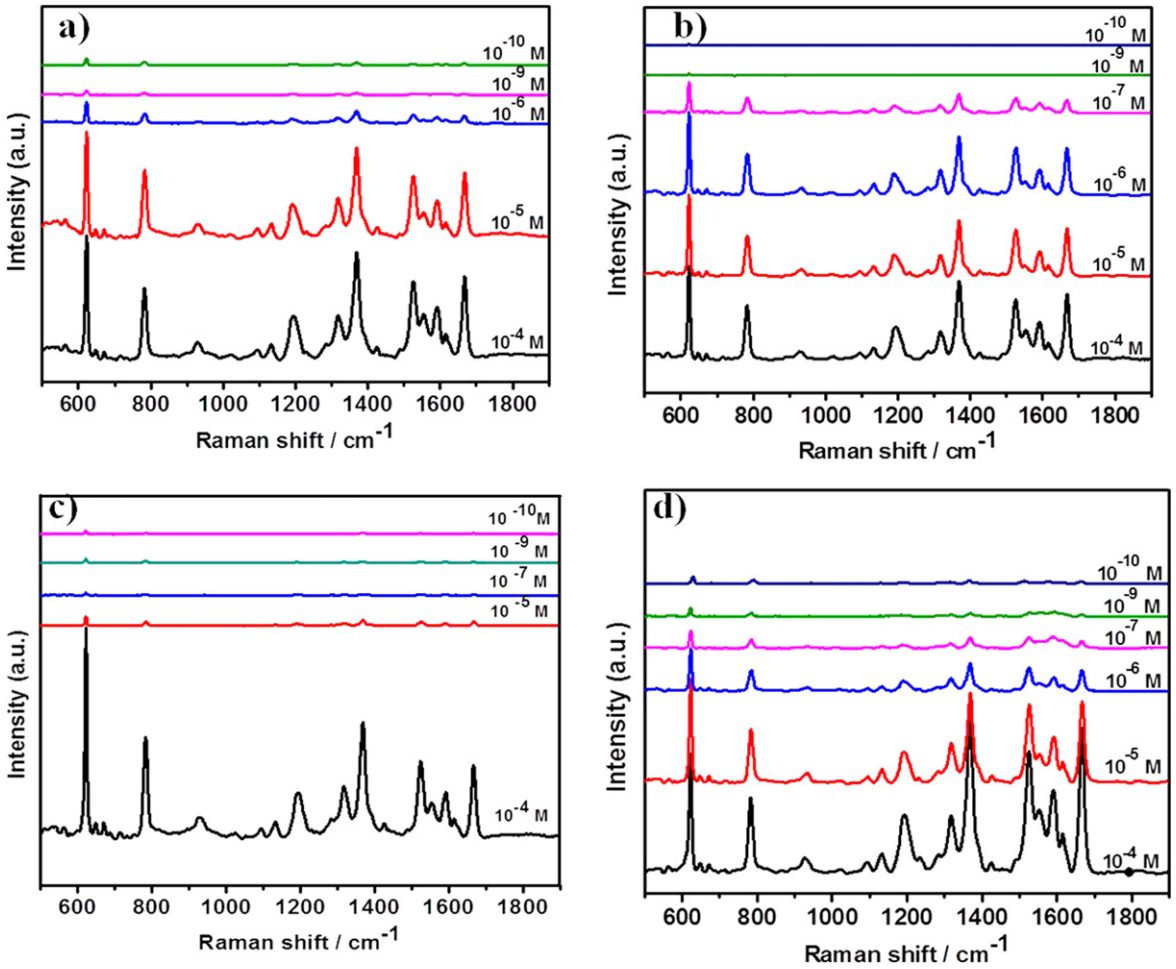

Figure 5. SERS spectra demonstrating the limit of detection (LoD) of all the samples (a) AgS13, (b) AgB13, (c) AgB25 and (d) AgS25.

addition to the enhancement due to large surface area, better localization of light in the cavities and lower electric field losses in GaN nanowalls. Further experiments are underway to probe the effect of size and position distribution of other metal nanoparticles on the sharp GaN nanowall network which may alter the SPR of the GaN nanowall network substrate also. Tuning of the band-edge emission energy by forming InGaN nanowall networks can also lead to better coupling to enhance the detection capability. This approach can significantly contribute to bio-molecular sensing for early stage detection of diseases like cancer, HIV, etc.

Acknowledgments

Authors thank Prof C N R Rao for his constant support and guidance.

References

[1] Cao Y, Jin R, Nam J-M, Thaxton C S and Mirkin C A 2003 *J. Am. Chem. Soc.* **125** 14676–7
[2] Xu L, Yan S-M, Cai C-B, Wang Z-J and Yu X-P 2013 *J. Anal. Methods Chem.* **2013** 201873
[3] Cao Y W C, Jin R and Mirkin C A 2002 *Science* **297** 1536
[4] Jarvis R M, Brooker A and Goodacre R 2004 *Anal. Chem.* **76** 5198–202
[5] Vo-Dinh T, Allain L R and Stokes D L 2002 *J. Raman Spectrosc.* **33** 511–6
[6] Martyshkin D V, Ahuja R C, Kudriavtsev A and Mirov S B 2004 *Rev. Sci. Instrum.* **75** 3
[7] Jin Y 2012 *Adv. Mater.* **24** 5135–65
[8] Kawabata A and Kubo R 1966 *J. Phys. Soc. Japan* **21** 1765–72
[9] Jain P K, Lee K S, Ivan H, El-Sayed and El-Sayed M A 2006 *J. Phys. Chem.* **110** 7238–48
[10] Albella P, Garcia-Cueto B, Gonz_alez F, Moreno F, Wu P C, Kim T-H, Brown A, O Everitt Y Y H and Videen G 2011 *Nano Lett.* **11** 3531–7
[11] Vigderman L and Zubarev E R 2012 *Langmuir* **28** 9034−9040
[12] Chen T, Pourmand M, Feizpour A, Cushman B and Reinhard B M 2013 *J. Phys. Chem. Lett.* **4** 2147−2152
[13] Jain P K and El-Sayed M A 2010 *Chem. Phys. Lett.* **487** 153–64
[14] Kumari G and Narayana C 2012 *J. Phys. Chem. Lett.* **3** 1130−1135
[15] Noguez C 2007 *J. Phys. Chem.* C **111** 3806–19
[16] Lance Kelly K, Coronado E, Zhao L L and Schatz G C 2003 *J. Phys. Chem.* B **107** 668–77
[17] Huang J-A, Zhao Y-Q, Zhang X-J, He L-F, Wong T-L, Chui Y-S, Zhang W-J and Lee S-T 2013 *Nano Lett.* **13** 5039–45

[18] Rout C S, Kumar A and Fisher T S 2011 *Nanotechnology* **22** 395704
[19] Cao Y W C, Jin R and Mirkin C A 2002 *Science* **297** 1536
[20] Haynes C L and Van Duyne R P 2001 *J. Phys. Chem.* B **105** 5599–611
[21] Wang R, Liu D, Zuo Z, Yu Q, Feng Z, Liu H and Xu X 2012 *J. Mater. Chem.* **22** 2410–8
[22] Nie B, Duana B K and Bohna P W 2012 *J. Raman Spectrosc.* **43** 1347–53
[23] Dar N, Wang W-J, Lee K-H and Chen I-G 2011 *Proc. 11th IEEE Conf. on Nanotechnology* p 297
[24] Siddhanta S, Thakur V, Narayana C and Shivaprasad S M 2012 *Appl. Mater. Interfaces* **4** 5807−5812
[25] Kesaria M, Shetty S and Shivaprasad S M 2011 *Cryst. Growth Design* **11** 4900
[26] Kesaria M and Shivaprasad S M 2011 *Appl. Phys. Lett.* **99** 143105
[27] Bhasker H P, Dhar S, Kesaria M, Sain A and Shivaprasad S M 2012 *Appl. Phys. Lett.* **101** 132109–13
[28] Thakur V, Kesaria M and Shivaprasad S M 2013 *Solid State Commun.* **171** 8–13
[29] Parisi J, Su L and Lei Y 2013 *Lab Chip* **13** 1501–8